



A Comparative Study of Chemical-Kinetic Mechanisms for Combustion of Methane/Hydrogen/Air Mixtures

Yuangang Wang¹ · Hee Sun Han¹ · Chae Hoon Sohn¹

Received: 25 April 2023 / Revised: 18 September 2023 / Accepted: 19 September 2023 / Published online: 16 October 2023
© The Author(s), under exclusive licence to The Korean Society for Aeronautical & Space Sciences 2023

Abstract

Eighteen chemical kinetic mechanisms for combustion of methane/hydrogen mixtures are compared for various burning conditions. The 18 mechanisms include eight detailed mechanisms, nine reduced mechanisms, and one global mechanism. Six of the reduced mechanisms are derived in this study. In the methane/hydrogen mixture, the blending ratio of hydrogen increases from 0 to 100% by 20% point in mole fraction. Calculated ignition delay times and laminar burning velocities are compared with available experimental data over the wide ranges of pressure and equivalence ratio as variables, respectively. Ignition delay times with NO₂ are also evaluated by several mechanisms to compare their prediction accuracy for NO_x emission. The aim of this study is to provide information for the purpose of choice of particular kinetic mechanism to obtain accurate results at a reasonable computational cost. The results show that although the reduced reaction mechanisms developed in this study have a narrower applicable range for predicting ignition delay times with hydrogen blending, they present higher accuracy in calculating laminar burning velocities and NO_x emissions.

Keywords Chemical mechanism · Ignition delay time · Laminar burning velocity · Hydrogen blending ratio · Pressure effect · NO_x emission

List of symbols

dt	Time difference
dT	Temperature difference
n_{H_2}	Hydrogen blending ratio
N	Number of data points
X_{H_2}	Hydrogen mole fraction
X_{CH_4}	Methane mole fraction

Exp.	Experimental
PFA	Path flux analysis
SP	Species

Abbreviations

ANN	Artificial neural network
CFD	Computational fluid dynamics
IDT	Ignition delay time
LBV	Laminar burning velocity
NG	Natural gas
Num.	Numerical

✉ Chae Hoon Sohn
chsohn@sejong.ac.kr

¹ Department of Mechanical Engineering, Sejong University, 209, Neungdong-ro, Gwangjin-gu, Seoul 05006, Republic of Korea

1 Introduction

With the increase in global energy demand and environmental concerns, search for clean and sustainable energy sources has become a major challenge [1–3]. Natural gas (NG), of which major component is methane (CH₄), has been recognized as a promising alternative to conventional fuels due to its low carbon and sulfur emissions and abundant reserves [4, 5]. However, due to slow laminar burning velocity (LBV) of NG, NG engines suffer from issues, such as low thermal efficiency and poor lean-burn capability [6]. In addition, the carbon emissions generated by methane combustion pose obstacles to achieving carbon neutrality. The addition of hydrogen (H₂) to CH₄–air mixtures has been proposed as a potential solution to improve the combustion performance of NG and to reduce CO₂ emissions. It can alter key combustion parameters, such as laminar flame speed,

flame thickness, flammability limits, and adiabatic flame temperature [6]. However, the use of 100% hydrogen is still immature technologically and logistically, and accordingly, hydrogen-enriched natural-gas applications could be a preliminary approach to facilitate the introduction of hydrogen. For this purpose, understanding the combustion characteristics of hydrogen and methane mixtures is crucial. Gas turbine operation typically occurs at pressures around 20 atm, with flame temperatures controlled at approximately 1500K under fuel-lean conditions. Therefore, it is necessary to analyze the combustion of hydrogen, methane, and air mixtures under a wide range of conditions, spanning from atmospheric to high pressures and from fuel-lean to fuel-rich conditions.

Furthermore, methane is an interesting propellant in terms of high-performance rocket engines and reusable rockets. Because demand for rocket launch at low cost is increasing, reusable rockets can be more viable in the future. Methane, as a propellant, has the advantages of easy storage and low cost over hydrogen, high specific impulse, and fewer coking problems than kerosene [7, 8]. It is suitable for the fuel of a reusable rocket engine. In this regard, simulating and analyzing the combustion characteristics of methane under various operating pressures are also important.

A large number of experimental results for combustion of hydrogen and methane have been published, and the accuracy of these experimental results is continuously improved. For example, Chen et al. compared the laminar flame speeds of hydrogen/methane/air mixtures at different equivalence ratios under atmospheric pressure through experiments in an early study [9]. Zhang et al. measured the ignition delay time of hydrogen/methane/oxygen/nitrogen mixtures using a shock tube with the highest hydrogen concentration in the mixture around 20% [10]. Later, Zhang et al. increased the hydrogen concentration up to 80% for three pressure conditions (5, 10, and 20 atm) [11]. Recently, more experimental results on the laminar flame speed of hydrogen and methane mixtures [12–14], experimental and computational results on ignition delay time [3, 15, 16], and results on changes in NOx emissions after hydrogen addition have been published [17, 18].

With experimental studies, accurate simulations using computational fluid dynamics (CFD) are necessary to explain relevant combustion phenomena [19, 20]. For simulations, selecting an appropriate chemical reaction mechanism for these simulations is crucial but still challenging, as it must balance the need for short computational time with accuracy in output parameters. Additionally, a lack of communication between kinetic scientists and CFD engineers can lead to poor mechanism selection. Therefore, expert assessments of kinetic mechanism must be provided for CFD engineers

to ensure that simulations incorporate the most suitable mechanisms. Zhang et al. evaluated 13 detailed kinetic mechanisms by comparing ignition delay times [21]. Ströhle et al. evaluated several detailed mechanisms for hydrogen combustion under gas turbine conditions, and they found that some of them show poor performance for the laminar flame speed at high pressures [22]. Kumar et al. also compared hydrogen–air reaction mechanisms used for unsteady shock-induced combustion devices [23]. Olm et al. have conducted comprehensive comparisons of hydrogen and syngas reaction mechanisms, identifying generally well-performing mechanisms as well as those that are only effective under specific conditions or for particular types of experiments [24, 25]. Zettervall et al. not only compared ignition delay times but also assessed four detailed mechanisms, seven reduced mechanisms, and six global mechanisms by calculating laminar burning velocities and strain rates [26]. However, these evaluations were conducted using methane rather than hydrogen–methane mixtures. The accuracy and computational efficiency of different mechanisms in simulating combustion of hydrogen–methane mixtures at various pressures and hydrogen blending ratios were not well evaluated. Currently, there are numerous available reaction models designed for high-fidelity CFD simulations, featuring a reduced number of species and elementary reactions. In most scenarios, the utilization of these reaction mechanisms presents no significant challenges. However, as pressure increases to relatively high values (20 atm) or as the hydrogen blending ratio surpasses certain thresholds (above 60%), errors in calculated results become more pronounced. Furthermore, while some reaction mechanisms yield accurate results, the absence of compiled reactions related to NOx emissions requires separate computations when applied in CFD simulations. Consequently, the creation of a reaction mechanism that encompasses NOx reactions and remains suitable for high-pressure and high-hydrogen-blending scenarios becomes imperative.

Therefore, the primary objective of this study is to guide in selecting reaction mechanisms for simulating the combustion of hydrogen–methane mixtures by evaluating existing and newly developed mechanisms. The secondary goal is to present reduced mechanisms developed in this study and validate their reasonability. For these purposes, the accuracy of the mechanisms is compared by calculating ignition delay times, laminar burning velocity, and NOx-related reactions under various simulation conditions ranging from low to high pressures and from 0 to 100% hydrogen blending ratios. Based on the simulation conditions and required computational time, recommendations for selecting the most appropriate mechanism are provided.

Table 1 Detailed mechanisms for CH₄/H₂/air mixture combustion included in the current evaluation

Type	No	Name	Year	Species	Steps	NO _x chemistry	Remarks
Detailed	1	NUIG 2020	2020	2746	11,279	o	C ₀ –C ₇ , Aromatic
	2	Aramco 2.0	2016	502	2716	x	C ₀ –C ₄
	3	CRECK CH ₄	2020	159	2459	o	C ₁ –C ₃ , Natural gas
	4	NUIG 2007	2007	118	663	x	C ₀ –C ₃
	5	USCII	2007	111	784	x	H ₂ /CO/C ₁ –C ₄
	6	San Diego	2016	68	311	o	CH ₄ , Natural gas
	7	GRI 3.0	1999	53	325	o	CH ₄ , Natural gas
	8	FFCM	2016	38	291	x	C ₀ –C ₂

2 Methodology

2.1 Kinetic Mechanisms

This section introduces commonly adopted mechanisms with different levels of complexity, which are classified as detailed, reduced, and global mechanisms in the descending order of complexity. Eight detailed mechanisms, nine reduced mechanisms, and one global mechanism are tested here.

2.1.1 Detailed Mechanisms

Detailed kinetic mechanisms adopted here are listed in Sect. 2.1.1. Table 1. All these mechanisms are validated using a wide range of experimental data, including ignition delay times, laminar burning velocity, and ignition of the mixtures with NO₂ species. As the state-of-the-art detailed mechanism, called NUIG Mech1.1 (NUIG 2020), is one of the most comprehensive mechanisms for C₀–C₇ species currently available. It includes 2746 species and was released by the NUI Galway research group in 2020 [27]. The same group also developed the mechanism of Aramco Mech. 2.0 (Aramco 2.0) including 502 species and was released in 2016 [28]. Aramco Mech 2.0 was built based on Aramco Mech 1.3 and has been developed to characterize the kinetic and thermochemical properties of a large number of C₁–C₄-based hydrocarbon and oxygenated fuels over a wide range of experimental conditions. The initial version of the NUI Galway model (NUIG 2007) consists of 118 species and 663 elementary reactions, which was published in the work of Petersen et al. in 2007 [29]. The CRECK CH₄ mechanism released in 2020 was developed by the chemical reaction engineering and chemical kinetics (CRECK) laboratory to simulate the reaction and properties of C₁–C₃ [30]. And, a H₂/CO/C₁–C₄ kinetic model, called USC Mech. version II (USCII), was developed by the research group of Wang et al. in 2007 [31]. This reaction model was subject to validation tests complying with reliable H₂/CO/C₁–C₄ combustion

data. Recently, Wang et al. and G. Smith at *SRI international* published another mechanism, called the foundational fuel chemistry model (FFCM) [32]. The FFCM can predict H₂, H₂/CO, CH₂O, and CH₄ combustion and includes 38 species and 291 steps. The combustion research group at UC San Diego developed the San Diego mechanism, which can simulate the combustion of methane or natural gas. The San Diego mechanism with nitrogen chemistry includes 68 species and 311 reactions [33]. And, the GRI 3.0 mechanism has been created by the Berkley combustion team as an updated version of GRI-Mech 2.11 [34]. It is a detailed kinetic mechanism for methane/air combustion including nitric species for NO_x predictions with 53 species and 325 reactions. In this study, a fuel mixture of hydrogen and methane is considered and the aforementioned eight detailed mechanisms are adopted to simulate combustion of the mixture.

2.1.2 Path Flux Analysis Method

Path flux analysis (PFA) reduction method is applied to reduce detailed chemical kinetic mechanisms [35]. Mechanism reduction aims to identify species that are important to the target species. The production and consumption fluxes of species are used to identify the important reaction pathways. The production and consumption fluxes, P_A and C_A , of species A can be calculated as follows:

$$P_A = \sum_{i=1, I} \max(v_{A,i} \omega_i, 0), \quad (1)$$

$$C_A = \sum_{i=1, I} \max(-v_{A,i} \omega_i, 0), \quad (2)$$

where $v_{A,i}$ is the stoichiometric coefficient of species A in the i th reaction. And ω_i is the net reaction rate of the i th reaction, respectively. I is the total number of elementary reactions. The flux of species A related with species B can be

calculated as

$$P_{AB} = \sum_{i=1, I} \max(v_{A,i} \omega_i \delta_B^i, 0), \quad (3)$$

$$C_{AB} = \sum_{i=1, I} \max(-v_{A,i} \omega_i \delta_B^i, 0), \quad (4)$$

$$\delta_B^i = \begin{cases} 1, & \text{if the } i\text{th elementary reaction involves species } B \\ 0, & \text{otherwise} \end{cases}. \quad (5)$$

Here, P_{AB} and C_{AB} denote, respectively, the production and consumption rates of species A due to the existence of species B . For example, when two generation fluxes are considered, the interaction coefficients for production and consumption of species A via B of first generation are defined as

$$r_{AB}^{\text{pro-1st}} = \frac{P_{AB}}{\max(P_A, C_A)}, \quad (6)$$

$$r_{AB}^{\text{con-1st}} = \frac{C_{AB}}{\max(P_A, C_A)}. \quad (7)$$

Using the production and consumption fluxes of the first generation, the interaction coefficients which are measures of flux ratios between A and B via a third reactant (M_i) for the second generation are defined as

$$r_{AB}^{\text{pro-2nd}} = \sum_{M_i \neq A, B} \left(r_{AM_i}^{\text{pro-1st}} r_{M_i B}^{\text{pro-1st}} \right), \quad (8)$$

$$r_{AB}^{\text{con-2nd}} = \sum_{M_i \neq A, B} \left(r_{AM_i}^{\text{con-1st}} r_{M_i B}^{\text{con-1st}} \right). \quad (9)$$

The summation here includes all possible reaction paths (fluxes) relating A and B . In theory, different threshold values can be set for different interaction coefficients. For simplicity, all the interaction coefficients can be lumped together and set only one threshold value

$$r_{AB} = r_{AB}^{\text{pro-1st}} + r_{AB}^{\text{con-1st}} + r_{AB}^{\text{pro-2nd}} + r_{AB}^{\text{con-2nd}}. \quad (10)$$

The coefficient defined above is used to evaluate the dependence/importance of species B to species A in the PFA method. The method can be extended to more generations and consumptions. Nevertheless, with the increase of the number of generations, the computation time is proportional to the species number. A more detailed explanation of the PFA method can be found in the study conducted by Sun et al. [35].

The PFA method has been developed into an in-house code program. To facilitate the simplification of reaction mechanisms, the following steps are taken:

1. Preparation of mechanism file: The detailed reaction mechanism file containing thermochemical data needs to be prepared for the mechanism that will undergo simplification.
2. Database generation for mechanism reduction: The database required for mechanism reduction is generated using tools like Senkin and perfectly stirred reactor (PSR) [36, 37]. This involves simulating conditions under which the reduced mechanism will be applied, including factors like pressure, temperature, and equivalence ratios.
3. Definition of target species: A set of target species is established to ensure that these selected species are retained and not eliminated during the reduction process.
4. Setting threshold values or interaction coefficients: After defining the target species, threshold values or interaction coefficients are set. This step plays a crucial role in the reduction process.
5. PFA method application: The PFA method is then employed to assess each species associated with the target species. If the calculated interaction coefficient is lower than the predetermined threshold value, the respective species is considered for elimination.

It's note worthy that the larger the threshold value, the smaller the reduced mechanism. This process results in a reduced reaction mechanism that retains essential combustion features while removing non-essential details.

2.1.3 Reduced and Global Mechanisms

In the present study, the target species are methane, hydrogen, oxygen, nitrogen, and their intermediate species produced in the reaction. The ranges of pressure, temperature, and equivalence ratio for mechanism reduction are from 1 to 20 atm, from 1000 to 2000 K, and from 0.5 to 1, respectively. It is important to emphasize that during the process of mechanism reduction, important species, elementary reactions, and their corresponding rate constants and coefficients have been retained. No modifications have been made to rate constants to artificially align the calculated results more closely with experimental data.

Reduced mechanisms are named according to the number of species, as shown in Table 2. Mechanism Nos. 1–4 and 6–7 are developed in the present study. The reduced mechanism No. 1, called SP282, contains 282 species. It is reduced from NUIG 2020 and kept all species related to reactions of methane and hydrogen as much as possible. The reduced mechanism No. 2, SP58, contains 58 species and it reduced the species number as much as possible while ensuring that the calculation results are consistent with the detailed mechanism NUIG 2020. Both SP282 and SP58 contain reaction mechanisms related to NO_x chemistry. The No.

Table 2 Reduced and global mechanisms for CH₄/H₂/air mixture combustion tested in this study

Type	No	Name	Year	Species	Steps	NO _x	Remarks
Reduced	1	SP282	2021	282	2025	o	NUIG 2020
	2	SP58	2021	58	506	o	NUIG 2020
	3	NO _x 56	2022	56	379	o	NUIG 2020 + GRI 3.0 NO _x
	4	NO _x 50	2022	50	258	o	Aramco 2.0 + GRI 3.0 NO _x
	5	USC50	2021	50	373	x	USCII
	6	SP41	2021	41	277	x	NUIG 2020
	7	SP33	2021	33	174	x	Aramco 2.0
	8	DRM22	2018	22	104	x	GRI 1.2
	9	DRM19	2018	19	84	x	GRI 1.2
	10	SG35	1991	16	35	x	Sydney/Yale/UCSD Workshop
Global	1	JLANN	2020	9	4	x	

6, SP41, is obtained after removing the NO_x chemical mechanism included in SP58. By combining the NO_x mechanism of GRI 3.0 with SP41, the mechanism No. 3, NO_x56, are developed. Another detailed mechanism, Aramco 2.0, is also used to generate the reduced mechanism, resulting in the mechanism No. 7, SP33. The SP33 does not include the NO_x mechanism. By adding the NO_x mechanism of GRI 3.0 to SP33, the reduced mechanism No. 4, NO_x50, is generated. It is important to make clear that the thermal data for non-NO_x reaction species in NO_x56 and NO_x50 are sourced from NUIG 2020 and Aramco 2.0, respectively, while the thermal data for species related to NO_x reactions are sourced from GRI 3.0. In conclusion, reduced mechanisms Nos. 1–4 contain NO_x mechanism, but Nos. 6 and 7 do not. The No. 5, USC50, was developed by D. Sharma et al. through the reduction of USCII, and it also does not include reactions related to NO_x [38].

The mechanism Nos. 8–10 are obtained from previous studies for comparison. The No. 8, DRM22, and No. 9, DRM19, [39, 40] were reduced from GRI 1.2 [41] using a reduction method proposed by Wang and Frenklach [42]. The DRM22 predicts high-temperature ignition delay times up to 10 atm and laminar flame properties up to 20 atm. Deviations from the original mechanism GRI 1.2 are between 1 and 10% with the largest deviation at high pressures. The DRM19 shows a larger deviation from the reference mechanism, in particular, for fuel-rich conditions. A widely used mechanism for methane/air combustion is the mechanism with 16 species and 35 irreversible reactions proposed by Smooke and Giovangigli (SG35) in 1991 [43] and constructed by selection of reactions from detailed reaction mechanisms available at that time. The mechanism was developed to model laminar flames and has been used in numerous published CFD modeling studies [44].

Global mechanisms result from crude simplification and are tuned to give accurate estimations of heat release, laminar flame propagation, fuel breakdown, and production of major species within a limited range of conditions [26]. A 4-step mechanism developed by Jones and Lindstedt, called JL, was extensively used in CFD simulations. In this study, its optimized version, called JLANN, developed by an artificial neural network (ANN) is adopted for a comparative study [45, 46]. The JLANN is obtained by ANN searching for the optimal reaction parameters that lead to the results matching those from GRI-Mech 3.0, the detailed mechanism for burning methane in a plug flow reactor [46].

2.2 Collection of Experimental Data

The mechanisms are evaluated by comparison with available experimental data. The ignition delay time (IDT), laminar burning velocity (LBV), and ignition delay time with NO₂ are selected as the validation targets. Experimental data are collected from reliable literature data to cover a range of conditions [11, 13, 26, 47–49]. They are selected by considering the fuel type, the hydrogen blending ratio, the range of operating pressure and temperature, and the equivalence ratio. For evaluation of IDTs and LBVs, the hydrogen blending ratio increases from 0 to 100% by 20% point. The operating temperature increases from 1000 to 2000 K at three operating pressures, 5, 10, and 20 atm in the case of evaluation of IDTs. Effects of hydrogen blending ratios and equivalence ratios are examined at 1 atm and temperature near 300 K for evaluation of LBVs. IDTs of the fuel with NO₂ are calculated to compare the accuracy of prediction of the mechanisms involving the NO_x steps in the aspect of the NO_x prediction. Three different pressures and the temperature range from 900 to 1900 K are considered. All of the experimental data and conditions are summarized in Table 3.

Table 3 Experimental validation data used in the present study

Property	Type	Fuel	H ₂ blending ratio (%)	Pressure [atm]	Temperature [K]	Equivalence ratio	Refs
Ignition delay time	Shock tube	CH ₄ /H ₂	0–100	5, 10, 20	1000–2000	0.5	Zhang et al. [11]
	Shock tube	CH ₄	0	10	1300–1900	0.5	Zettervall et al. [26]
Laminar burning velocity	Various devices	H ₂	100	1	293	0.4–3.2	Teng [14]
		CH ₄ /H ₂	0–80	1	303	0.6–1.8	Zhang et al. [13]
Ignition with NO ₂	Shock tube	CH ₄	0	1, 5, 10, 20	298	0.6–1.4	Amirante et al. [49]
		H ₂	1	1.6, 13, 33	900–1900	0.5	Mathieu et al. [47]
		O ₂	1				
		NO ₂	0.16				
		Ar	97.84				

2.3 Details on Modeling

The hydrogen blending ratio (n_{H_2}) is defined as the mole percentage of hydrogen in the CH₄/H₂ mixtures. It is calculated by the equation

$$n_{H_2} = \frac{X_{H_2}}{X_{H_2} + X_{CH_4}} \times 100\%, \quad (11)$$

where n_{H_2} denotes hydrogen blending ratio, X_{H_2} hydrogen mole fraction in the mixture, and X_{CH_4} methane mole fraction in the mixture.

A comprehensive software package [50] is used to simulate laminar premixed flames and ignition delays. Ignition in a closed homogeneous reactor is modeled using a constant volume approach with an energy equation solved. The ignition delay time is determined by the instant when time derivative of temperature, dT/dt , has its maximum. The experimental results used for comparison in this study are obtained from the previous study [11]. In the previous study, pressure generated by the reflected shock wave in the shock tube increased at a rate of 4%/ms after 1.5 ms due to the facility-dependent boundary layer effect. Therefore, when calculating the ignition delay in the present study, the same increase rate of pressure is set after 1.5 ms.

Laminar flames are simulated using the premixed-flame model with adaptive grids, where solution gradient and curvature are set to 0.02 and 0.03, respectively. It resulted in grid-independent solutions for all mechanisms [26]. To calculate the LBFs, the equivalence ratio, ϕ , covers from fuel-lean ($\phi = 0.6$) to fuel-rich ($\phi = 1.4$) conditions along with a specified initial inlet temperature of 300 K. In the present work, the “multi-component transport” is chosen,

because it can accurately predict the laminar burning velocities [51]. In addition, a thermal diffusion coefficient, called the Soret effect, is included, which is significant for light species, such as H and H₂. Details on the different approaches to transport model can be found in the literature [50]. One should keep in mind that transport treatment becomes increasingly significant as the diameter of species decreases and, therefore, larger deviations is expected for hydrogen flames [26].

The agreement between experimental data and calculation results is evaluated using the following parameter:

$$\text{Discrepancy (\%)} = \frac{1}{N} \sum_{i=1}^N \frac{\text{abs(Num.}_i - \text{Exp.}_i)}{\text{Exp.}_i} \times 100\%, \quad (12)$$

where N is the number of data points, and Num. and Exp. are numerical and experimental results, respectively. For example, when the ignition delay time is calculated as temperature increases at 5 atm with a hydrogen blending ratio of 0%, N will be the number of temperature points. To clearly compare the errors across all cases, the discrepancy is normalized by the minimum in all the cases. The critical threshold for evaluating the accuracy of computational results with various reaction mechanisms is set to be 15%. The value of 15% was determined based on a comprehensive comparison of all calculation results. This value can help to distinguish between the detailed and reduced mechanisms and can also do between various reaction mechanisms based on their computational results.

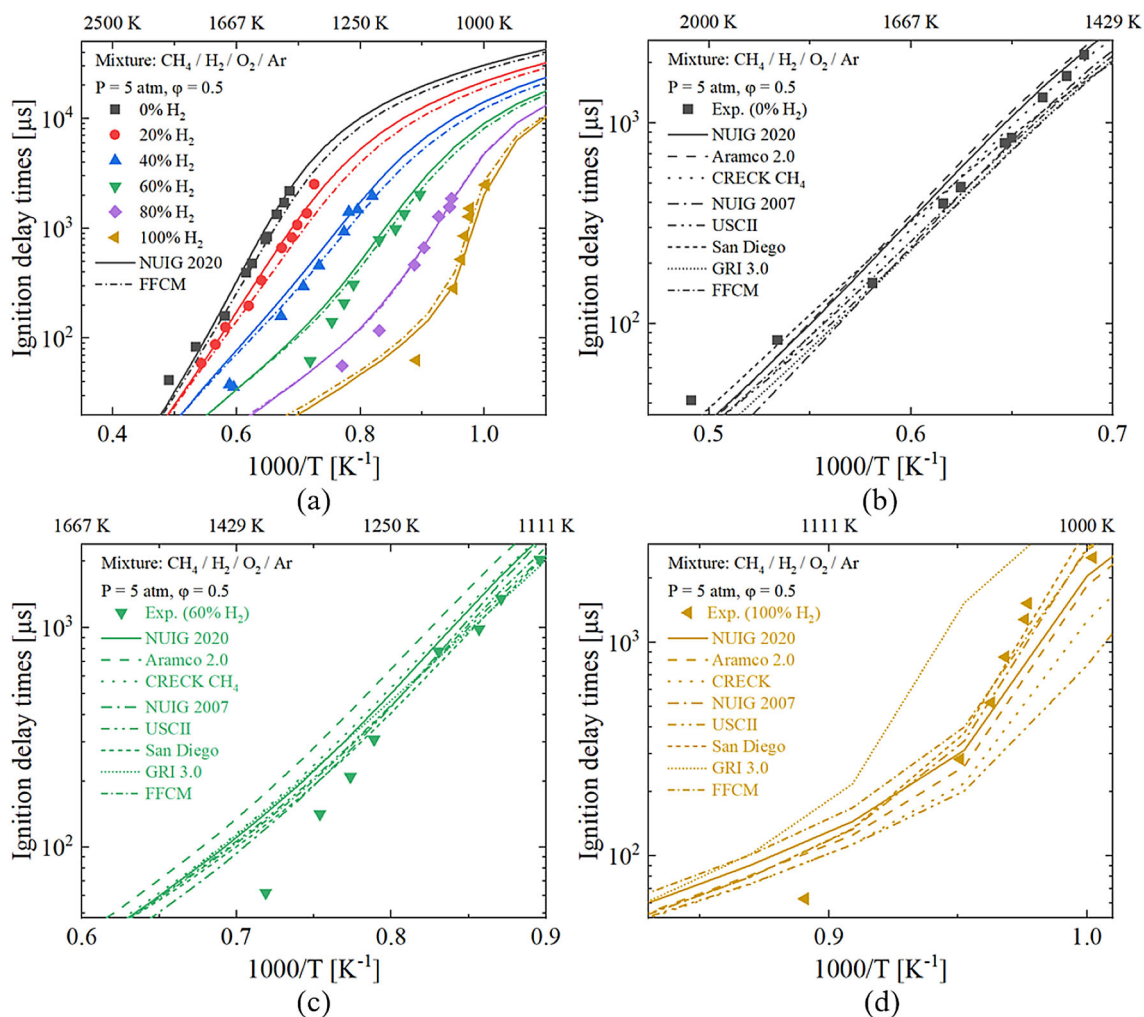


Fig. 1 a Errors between predicted ignition delay time and experimental data over the broad H_2 blending ratios at equivalence ratio of 0.5 and 5 atm. Enlarged views of comparison at blending ratios of b 0%, c 60%, and d 100%. Symbols: experimental data; lines: calculated data in this work

3 Results and Discussion

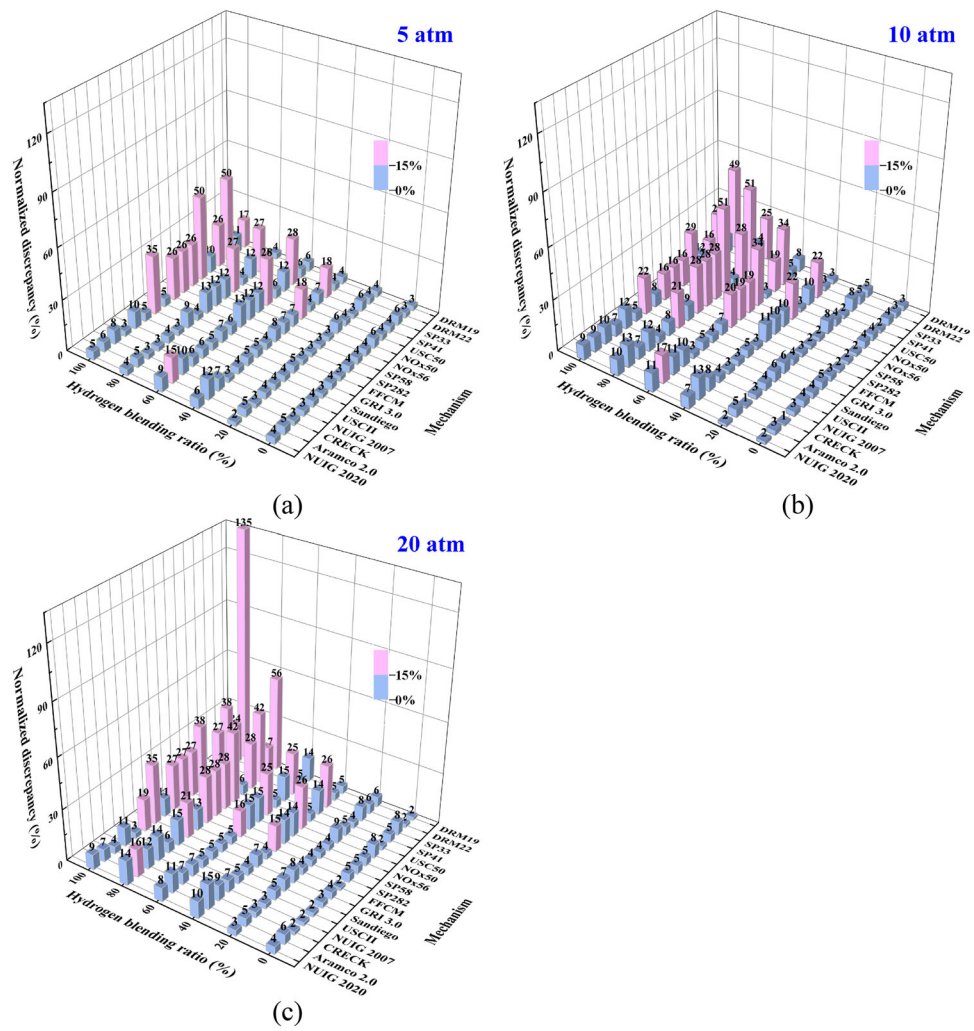
3.1 Ignition Delay Time

Ignition delays of lean methane–hydrogen mixtures (equivalence ratio of 0.5) with hydrogen fractions from 0 to 100% are compared in the temperature range from 1000 to 2000 K and the pressure range from 5 to 20 atm. All the reaction mechanisms listed in Tables 1 and 2 are adopted in the calculation. Since the trend of ignition delay is consistent at all pressures, the calculation results at 5 atm are chosen as an example for this comparative study, as shown in Fig. 1. It is seen that the ignition delays decrease with increasing n_{H_2} due to high reactivity, high diffusion, and low auto-ignition temperature of H_2 . The results calculated with the detailed reaction mechanisms of NUIG 2020 and FFCM are presented in Fig. 1a. It is found that both reaction mechanisms show a good agreement with experimental results for all the hydrogen blending

ratios. The calculation results of the other detailed reaction mechanisms can be checked in Fig. 1b–d. With the increase of n_{H_2} , the error increases even if the results are calculated by a detailed mechanism. When the n_{H_2} is 100%, it can be clearly seen that the calculation errors of GRI 3.0 are relatively large. The calculation results of the reduced reaction mechanisms are not shown here and their discrepancies will be compared with the detailed reaction mechanism in a later section.

Figure 2 shows the discrepancy between calculated ignition delays and experimental results for all the reaction mechanisms as pressure and n_{H_2} increase. Each discrepancy value was obtained by comparing the calculated ignition delay results with experimental data in the temperature range of 1000–2000 K. Figure 2a shows that at relatively low pressures (5 atm), the detailed reaction mechanism provides higher calculation accuracy compared to the reduced mechanism. As n_{H_2} increases from 0 to 100%, only the detailed

Fig. 2 Normalized discrepancy between predicted ignition delay time and experimental data over the broad blending ratio at pressures of **a** 5 atm, **b** 10 atm, and **c** 20 atm



reaction mechanisms of Aramco.2.0 and GRI 3.0 exhibit discrepancies above 15% under certain conditions. However, in the reduced mechanisms, SP33 and NOx50 show a discrepancy of 18% starting from a blending ratio of 40%, which gradually increases to 50% as n_{H_2} increases up to 100%. The discrepancies for SP282, SP58, NOx56, and SP41 also exceed 15% when n_{H_2} reaches 100%. The DRM19 and DRM22 published in previous studies also show a high discrepancy when n_{H_2} is 100%; however, their discrepancy is relatively low when n_{H_2} increases up to 80%. As the pressure increases to 10 atm and shown in Fig. 2b, the calculated discrepancies exceed 15% at smaller blending ratios. For example, at a blending ratio of 80%, the calculated discrepancy for GRI 3.0 is 21%, which is higher than the 9% discrepancy at 5 atm. Also, the discrepancies of SP282, SP58, NOx50, and SP41 exceed 15% when n_{H_2} is 60%. As the pressure is increased to 20 atm, the discrepancy of the reduced mechanism further increases, starting from n_{H_2} of 40%. Additionally, the detailed reaction mechanisms also show discrepancies approaching 15% at the blending ratio

of 80%. Consequently, the operational range of the reaction mechanisms to accurately calculate the IDT becomes narrower with pressure. The results for SG35 and JLANN are not presented in Fig. 2 due to their inability to provide reasonable results for ignition delay time calculations.

3.2 Laminar Burning Velocity

Figure 3 shows the errors between the calculated and experimental results of laminar burning velocity at 1 atm and 300 K as an example. It demonstrates how the laminar burning velocity varies with the equivalence ratio and n_{H_2} . The equivalence ratio ranges from 0.6 to 1.8 with a step size of 0.1, while n_{H_2} increases from 0 to 100% with a step size of 20%. From Fig. 3a, it can be observed that the laminar burning velocity first increases and then decreases as the equivalence ratio increases. Furthermore, as n_{H_2} increases, the equivalence ratio corresponding to the maximum laminar burning velocity also gradually increases. This trend is

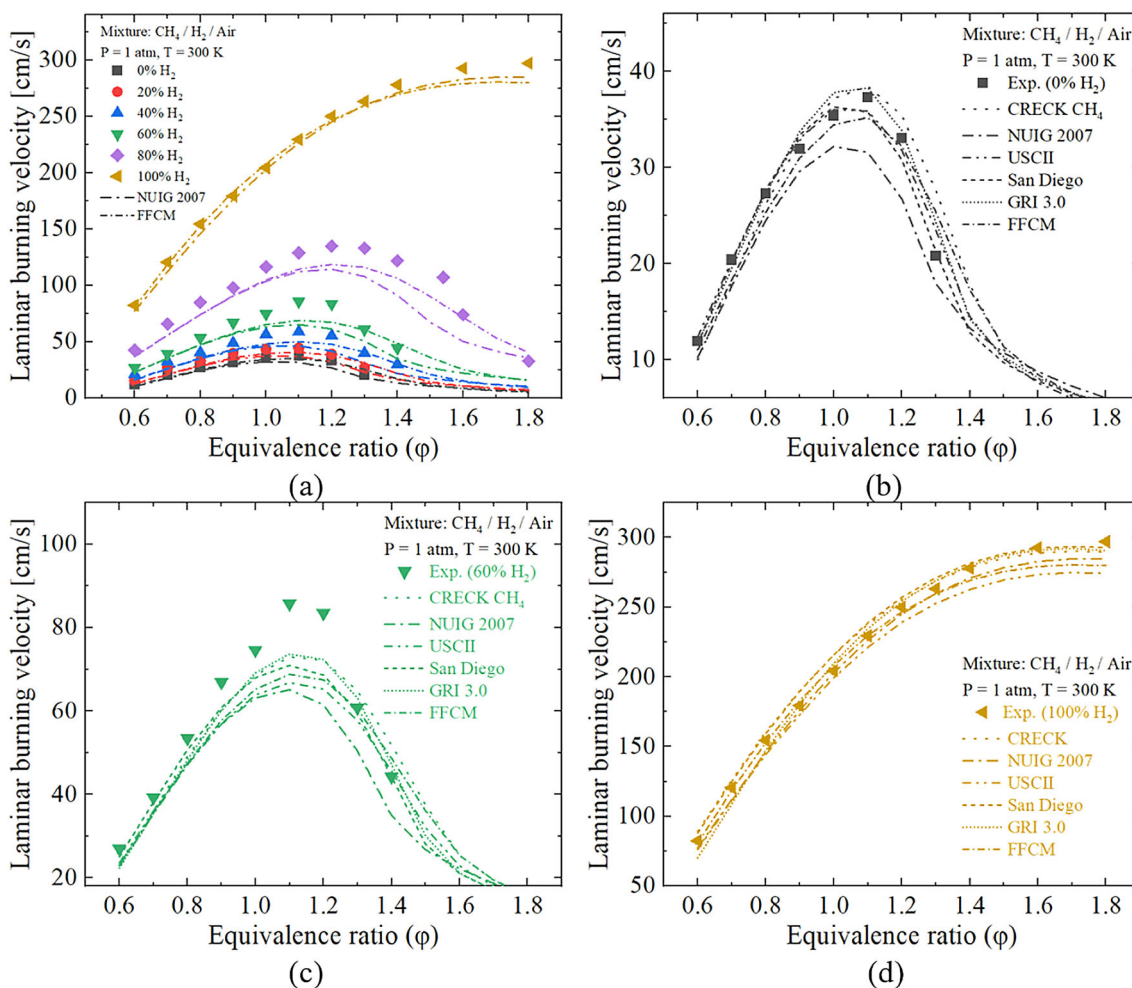
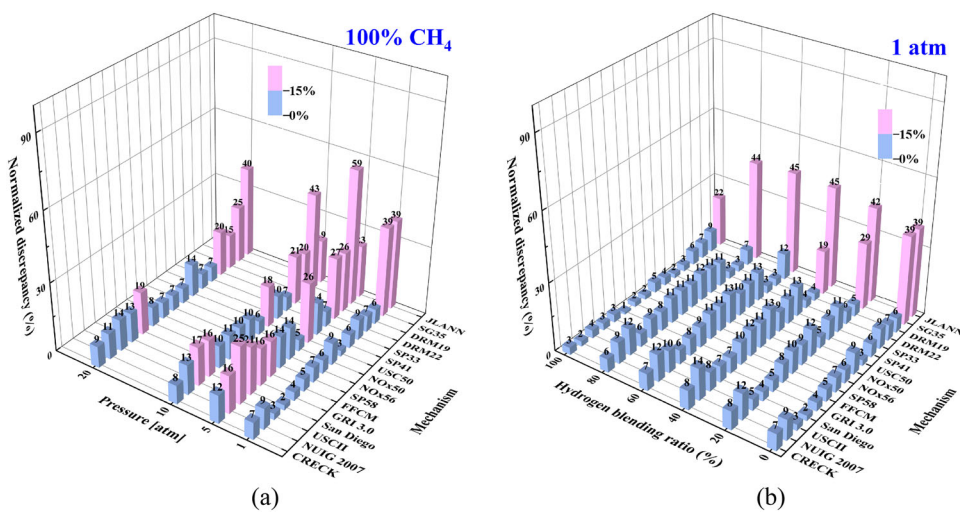


Fig. 3 a Errors between predicted laminar burning velocity and experimental data as H₂ blending ratios increases at 300 K and 1 atm. Zoomed-in views of comparison shown for blending ratio **b** 0%, **c** 60%, and **d** 100%. Symbols: experimental data; lines: calculated data in this work

Fig. 4 The normalized discrepancy between predicted laminar burning velocity and experimental data calculated **a** with pressure at n_{H_2} of 0% and **b** with the blending ratio at 1 atm



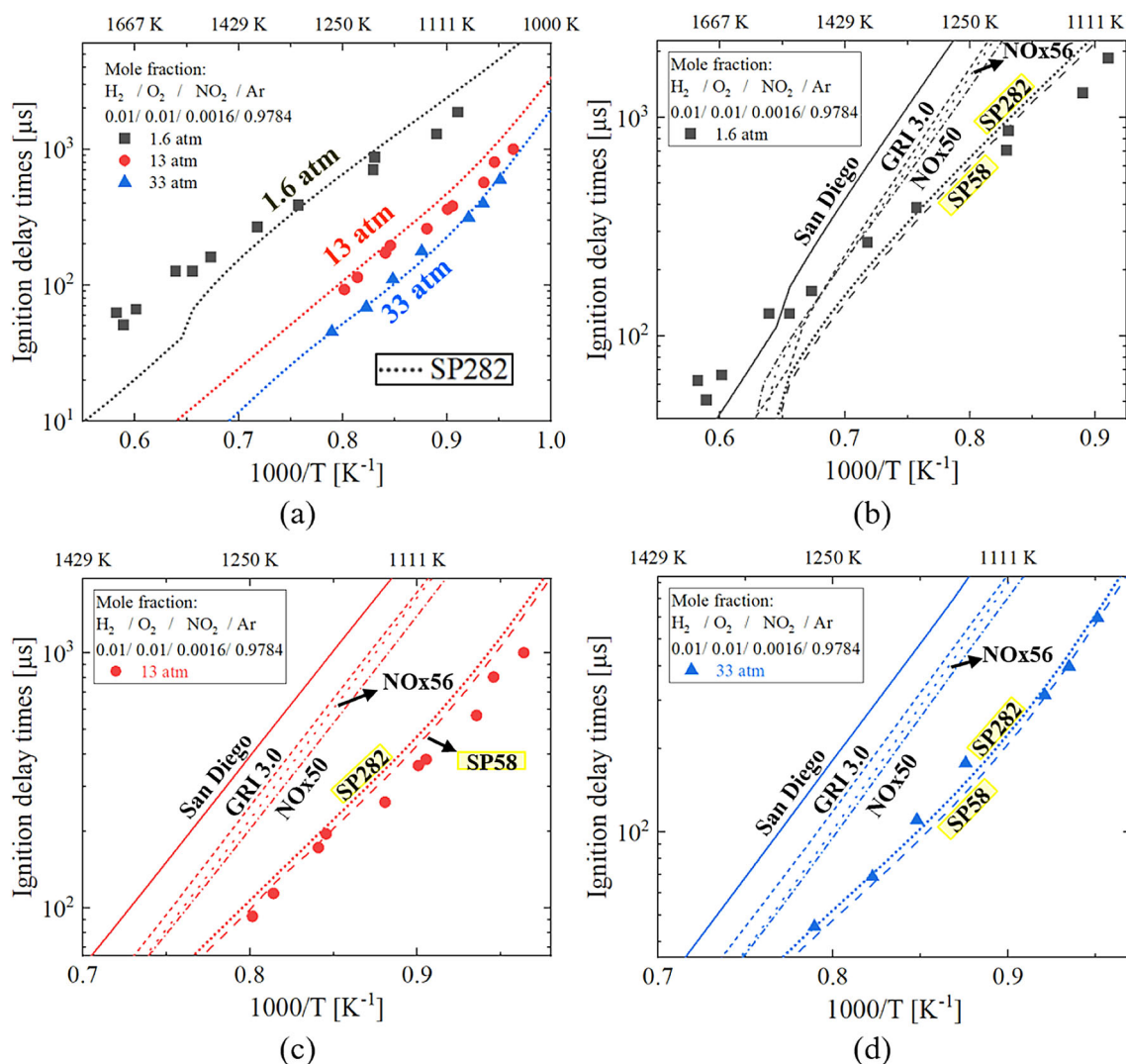


Fig. 5 a Errors between calculated ignition delay time with NO_2 and experimental data at various pressures using the reduced mechanism, SP282. Comparison of experimental data and predicted results by San

Diego, GRI 3.0, SP282, SP58, NOx56, and NOx50 at the pressure of **b** 1.3 atm, **c** 13 atm, and **d** 33 atm. Symbols: experimental data; lines: calculated data in this work

the most evident at n_{H_2} of 100%, where the laminar burning velocity continues to increase even when the equivalence ratio is increased to 1.8. As predicted, if the equivalence ratio continues to increase, the laminar burning velocity will gradually decrease, which has been already shown in the previous studies [48]. Figure 3b–d shows the zoomed-in results for hydrogen blending ratios of 0%, 60%, and 100%, respectively. It is seen that the calculated results by all detailed reaction mechanisms are relatively accurate when the hydrogen blending ratio is 0% or 100%. However, when n_{H_2} is 60%, the error is relatively large, as will be shown in more detail in the following paragraph. It should be noted that in this study, the laminar burning velocity is compared at four pressure conditions of 1, 5, 10, and 20 atm for pure methane. Although the results are not displayed in Fig. 3, the

errors between the calculated and experimental results will be shown later.

The discrepancy comparison of laminar burning velocity is shown in Fig. 4. Figure 4a displays the errors between calculated results and experimental data at different pressures for the 100% methane. At 1 atm, only the reduced mechanism, SG35, and the global mechanism, JLANN, have large errors, while the errors of the other detailed reaction mechanisms are less than 10%. When the pressure increases to 5 atm, except for CRECK, the errors of the other detailed reaction mechanisms increase over 15%. Due to long calculation times, complete results for NUIG 2020 and Aramco2.0 were not obtained. However, the reduced mechanisms of SP33, SP41, SP58, NOx50, and NOx56 derived from the two detailed mechanisms show small errors, even at high

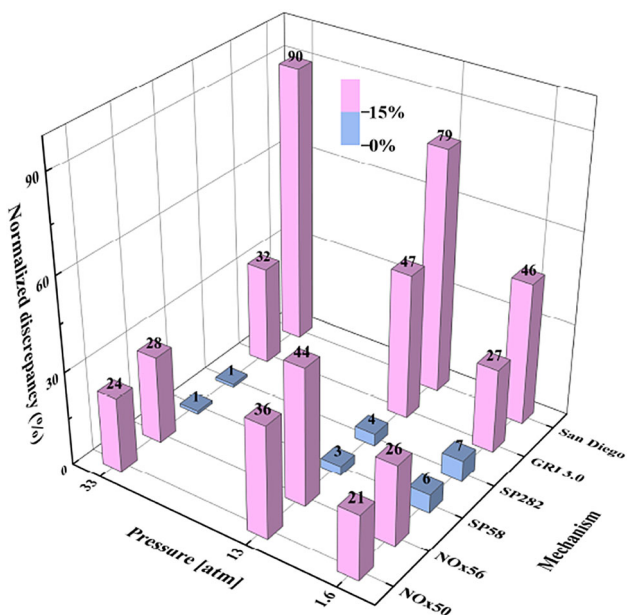


Fig. 6 Normalized discrepancy between predicted ignition delay time with NO₂ and experimental data calculated at several pressures

pressures of 10 and 20 atm. This indicates that the original detailed reaction mechanisms NUIG 2020 and Aramco 2.0 should be also accurate. Figure 4b shows the discrepancy between calculated results and experimental data as n_{H_2} increases from 0 to 100% at 1 atm. It is seen that all the detailed reaction mechanisms give accurate results. Only the detailed reaction mechanism of NUIG 2007 and the five reduced reaction mechanisms developed in this study have slightly larger discrepancy, but the errors do not exceed 15%. In contrast to the results with pressure variation, DRM19 and DRM22 give good results for all hydrogen mixture fractions.

Both the reduced mechanism of SG35 and the global mechanism of JLANN showed relatively large discrepancies in predicting ignition delay times and laminar burning velocities. The laminar burning velocities is not calculated by using NUIG 2020 here, because it requires a significant amount of computational time. The results from NUIG 2020 can be predicted from that of NUIG 2007, as both share the same reaction mechanisms for methane and hydrogen.

3.3 Ignition Delay Time with NO₂

Next, the calculation discrepancy of reaction mechanisms containing NOx in terms of ignition delay time of hydrogen–oxygen mixtures containing NO₂ is examined. NO₂ of 1600 ppm is added to the hydrogen–oxygen mixture, and argon is used as a diluent gas. Ignition delay times calculated using six reaction mechanisms are compared at three pressures of 1.6, 13, and 33 atm. The six reaction mechanisms are GRI 3.0, San Diego, and four reduced mechanisms containing NOx developed in this study, i.e., SP282, SP58, NOx56, and NOx50. The experimental results used for a comparative study are from the literature [47]. From Fig. 5a, it is seen that the calculation results of SP282, which has the most species, are quite accurate, especially at high pressure. When comparing the results at each pressure separately, Fig. 5 shows that the mechanism, SP58, which is also reduced from NUIG 2020, has similar calculation results to those of SP282 at all pressures. On the other hand, the other four mechanisms show significant errors.

The comparison of the results calculated by each mechanism and experimental data is presented in Fig. 6. It is seen that the performance of the reduced mechanisms developed in this study is excellent when it comes to NOx-related calculations with the average error of only 1% at 33 atm. On the

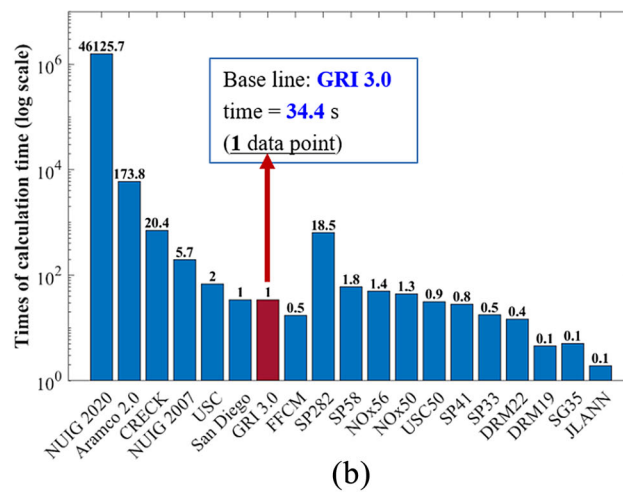
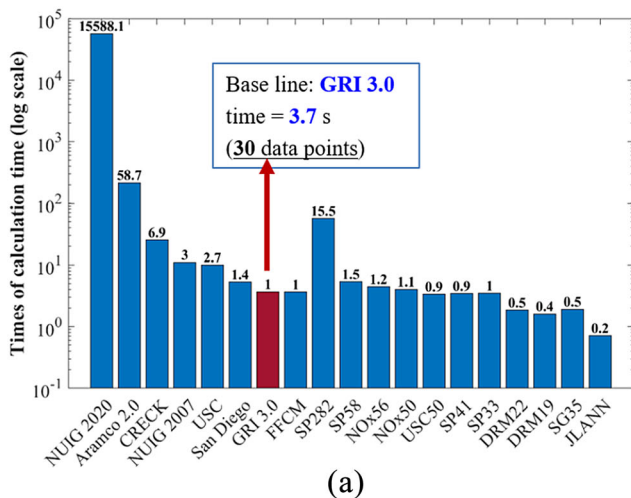


Fig. 7 Comparison of computational time taken to obtain a 30 data points of ignition delay time and b one data point of laminar burning velocity

Table 4 Summary of results calculated by detailed mechanisms, including a comparison of the discrepancy in ignition delay time (IDT) and laminar burning velocity (LBV), a comparison of the ignition delay time considering NO₂, as well as the comparison of computation time

Detailed mechanisms		Pressure [atm]	Discrepancy in IDT between simulations and experiments					Discrepancy in LBV 100% CH ₄	Ignition with NO ₂	Computational time	
Name	# of Species		0% H ₂	20%	40%	60%	80%			100%	IDT
NUIG 2020	2746	1							O	15,588	46,126
		5									
		10									
		20									
Aramco 2.0	502	1							X	59	640
		5									
		10									
		20									
CRECK CH ₄	159	1							O	7	20
		5									
		10									
		20									
NUIG 2007	118	1							X	3	6
		5									
		10									
		20									
USC II	111	1							X	2.7	2
		5									
		10									
		20									
San Diego	68	1							O	1.4	1
		5									
		10									
		20									
GRI 3.0	53	1							O	1 (base)	1 (base)
		5									
		10									
		20									
FFCM	38	1							X	1	0.5
		5									
		10									
		20									

"O" indicates the inclusion of NO_x mechanisms, while "X" indicates their exclusion. Blue color means the discrepancy less than 15%; red color means the discrepancy greater than 15%

other hand, the other two mechanisms developed in this study and the two widely used mechanisms have relatively larger errors. The NO_x-related reactions selected for the development of NO_x50 and NO_x56 are all from GRI 3.0, while a large part of the NO_x-related reactions in San Diego is the same as those in GRI 3.0. This result also indicates that the NO_x-related reactions in GRI 3.0 and San Diego are not sufficient in simulating pressure dependence accurately.

3.4 Computational Time

Finally, computational time of each mechanism is compared. The calculations are conducted using 32 CPU cores with a clock frequency of 3.5 GHz. All the results are normalized by the computational time of GRI 3.0. As shown in Fig. 7, the required time for both ignition delay time and laminar flame speed calculations is positively correlated with the number of species in the reaction mechanism. Figure 7a shows the required time for computing 30 ignition delay times using different mechanisms, with a required time of 3.7 s with GRI 3.0. The detailed reaction mechanism of NUIG 2020

requires 15,588 times longer than the computational time of GRI 3.0, while the computational times of the other mechanisms developed in this study are similar to that of GRI 3.0, except for SP282, which required 15.5 times longer than the computational time of GRI 3.0. Figure 7b shows the required time for computing one data of laminar flame speed, with a required time of 34.4 s for GRI 3.0. The required time of NUIG 2020 is 46,125 times longer than that of GRI 3.0. This is also the reason why calculation of the laminar flame speed using NUIG 2020 was not conducted. It is due to its excessively long computational time. These results indicate that when selecting a reaction mechanism, both accuracy and computational time should be taken into account. It is recommended that a mechanism with the shortest computational time within an acceptable range of error is selected.

Table 5 Summary of results calculated by reduced mechanisms

Reduced mechanisms		Pressure [atm]	Discrepancy in IDT between simulations and experiments					Discrepancy of LBV 100% CH ₄	Ignition with NO ₂	Calculation time	
Name	# of Species		0% H ₂	20%	40%	60%	80%			100%	IDT
SP282	282	1							O	15.5	18.5
		5									
		10									
		20									
SP58	58	1						O	1.5	1.8	
		5									
		10									
		20									
NOx56	56	1						O	1.2	1.4	
		5									
		10									
		20									
NOx50	50	1						O	1.1	1.3	
		5									
		10									
		20									
USC50	50	1						X	0.9	0.9	
		5									
		10									
		20									
SP41	41	1						X	0.9	0.8	
		5									
		10									
		20									
SP33	33	1						X	1	0.5	
		5									
		10									
		20									
DRM22	22	1						X	0.5	0.4	
		5									
		10									
		20									
DRM19	19	1						X	0.4	0.1	
		5									
		10									
		20									
JLANN (Global)	9	1						X	0.2	0.1	
		5									
		10									
		20									

4 Summary of Numerical Errors or Discrepancies

All the above calculation results are summarized and presented in Tables 4 and 5. Table 4 shows the results calculated by the detailed chemical mechanisms. While pressure and hydrogen blending ratio are variable, the ignition delay time results calculated by detailed mechanisms are quite accurate (with an error of less than 15%). Only Aramco 2.0, GRI 3.0, and San Diego exhibit higher errors at some high pressures or high-hydrogen-blending ratios. The mechanisms of NUIG 2007, USC II, and San Diego show significant errors in calculating laminar burning velocity at 5 atm and 10 atm. In most cases, a detailed reaction mechanism can be used to calculate and simulate combustion of methane and hydrogen mixture. The selection should be made reasonably based on the required computational time and whether NO_x needs to be considered or not.

Table 5 summarizes the results of reduced reaction mechanisms. Compared with the detailed reaction mechanism, the reduced reaction mechanism generally exhibits larger calculation errors in predicting ignition delay times at pressures above 10 atm and hydrogen mixing ratios above 40%. In terms of calculation of laminar burning velocities, the six reduced reaction mechanisms developed in this study show high accuracy, with discrepancies below 15%. It is worth noting that the reduced mechanisms of SP282 and SP58 show higher accuracy than GRI 3.0 and San Diego in calculating reactions of NO_x emissions. However, the computational times are longer by about 15.5 times and 1.5 times compared to GRI 3.0, respectively. Furthermore, across all pressure and hydrogen blending ratio ranges, the reduced mechanism USC50 demonstrates a similar high level of accuracy as observed with the detailed mechanism USCII.

5 Conclusions

Various chemical kinetic mechanisms for burning of methane/hydrogen mixtures are tested for various burning conditions. The numerical results show that the widely used GRI-Mech 3.0 works well when the pressure is less than 10 atm and the blending ratio is less than 60%. If the simulation is performed above 10 atm and the blending ratio exceeds 60%, a detailed reaction mechanism with more species, such as San Diego mechanism, should be adopted, although longer computational time is required. If calculation of NO_x emissions is not considered, the FFCM is a good choice under various operating conditions. The reduced mechanism of SP58 has higher accuracy in calculating NO_x emission, but the computational time is 1.5 times longer than that of GRI 3.0. In the range of 1–20 atm, the laminar burning velocity of methane calculated using the reduced reaction mechanism developed in this study is more accurate than those calculated using the detailed mechanisms San Diego, GRI 3.0, and USC II.

When selecting a reaction mechanism, it is important to consider the reaction characteristics depending on the simulation purpose. For example, ignition delay time is more important for study of ignition in high-speed propulsion, while more consideration is needed for laminar burning velocity when simulating hydrogen combustion in a gas turbine combustor. Additionally, it is necessary to check the required computation time. In studying pollutant emissions, the accuracy of NO_x-related reaction calculations is also critical.

In future works, the reduced reaction mechanisms will be applied to CFD simulations and compared with the existing detailed mechanisms. This comparison aims to validate the accuracy of the reduced reaction mechanisms in simulating methane and hydrogen combustion.

Acknowledgements This work was supported by Korea Institute of Energy Technology Evaluation and Planning (KETEP) grant funded by the Korea government (MOTIE) (20206710100030, Development of Eco-friendly GT Combustor for 300MWe-class High-efficiency Power Generation with 50% Hydrogen Co-firing).

Declarations

Conflict of interest On behalf of all authors, the corresponding author states that there is no conflict of interest.

Appendix A: Errors between predicted results and experimental data

The errors between predicted results and experimental data not depicted in Figs. 1, 3, and 5 are shown in this appendix section.

A.1 Ignition Delay Time

The comparison between the predicted ignition delay times and experimental results for the hydrogen blending ratio ranging from 0 to 100% at an equivalence ratio of 0.5, and pressures of 5 atm, 10 atm, and 20 atm is presented in Figs. 8, 9, and 10, respectively.

A.2 Laminar Burning Velocity

The comparison between the predicted laminar burning velocities and experimental data for the hydrogen blending ratio ranging from 0 to 100% at equivalence ratios of 0.6–1.8, and pressures of 1 atm is presented in Fig. 11. The comparison between the predicted results and experimental data for 100% methane combustion at equivalence ratios of 0.6–1.8 and 1 atm is shown in Fig. 12.

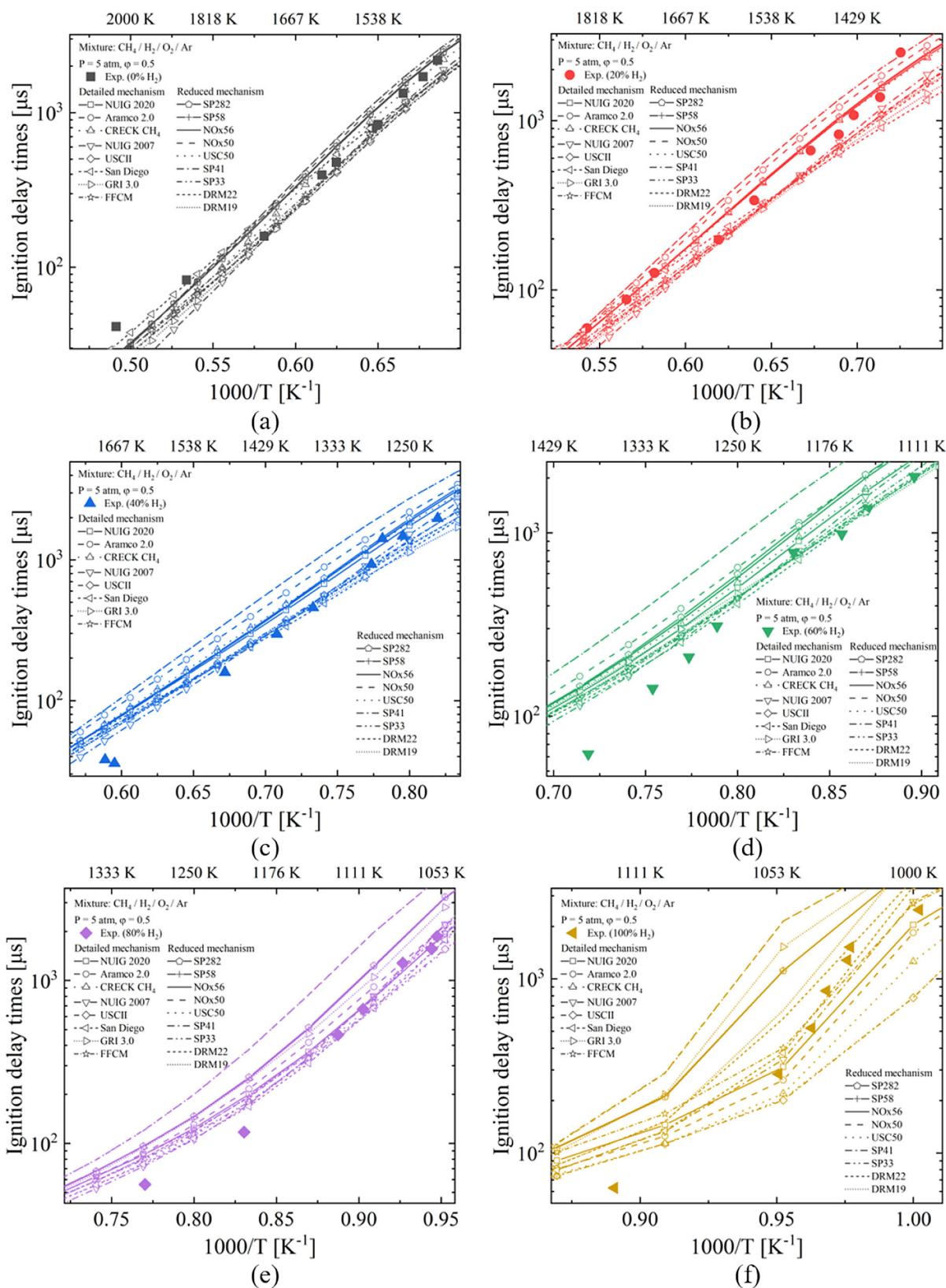


Fig. 8 Errors between predicted ignition delay time and experimental data for the H_2 blending ratios: **a** 0%, **b** 20%, **c** 40%, **d** 60%, **e** 80%, and **f** 100% at an equivalence ratio of 0.5 and 5 atm. Symbols: experimental data; lines: calculated data in this work

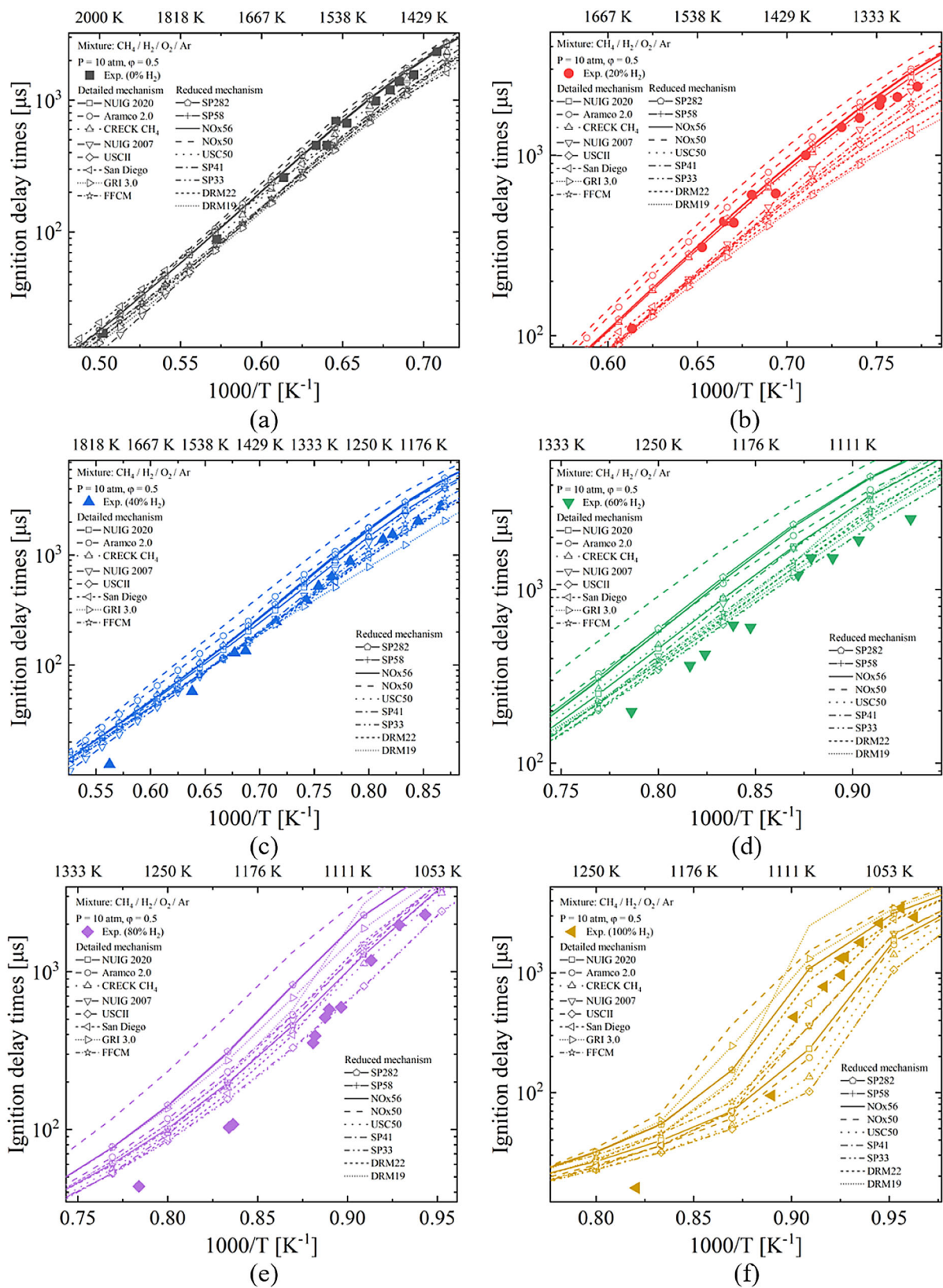


Fig. 9 Errors between predicted ignition delay time and experimental data for the H_2 blending ratios: **a** 0%, **b** 20%, **c** 40%, **d** 60%, **e** 80%, and **f** 100% at an equivalence ratio of 0.5 and 10 atm. Symbols: experimental data; lines: calculated data in this work

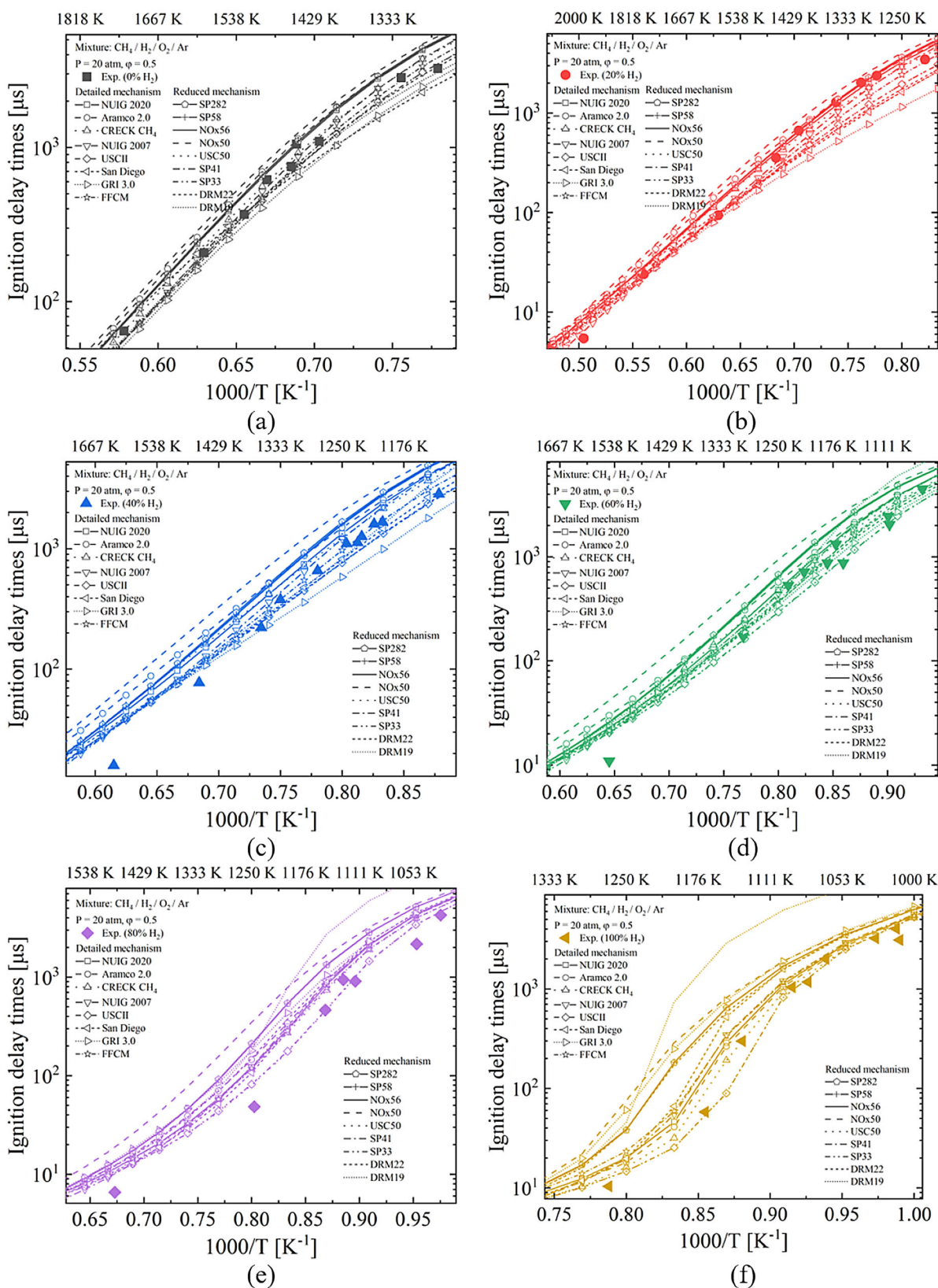


Fig. 10 Errors between predicted ignition delay time and experimental data for the H₂ blending ratios: **a** 0%, **b** 20%, **c** 40%, **d** 60%, **e** 80%, and **f** 100% at an equivalence ratio of 0.5 and 20 atm. Symbols: experimental data; lines: calculated data in this work

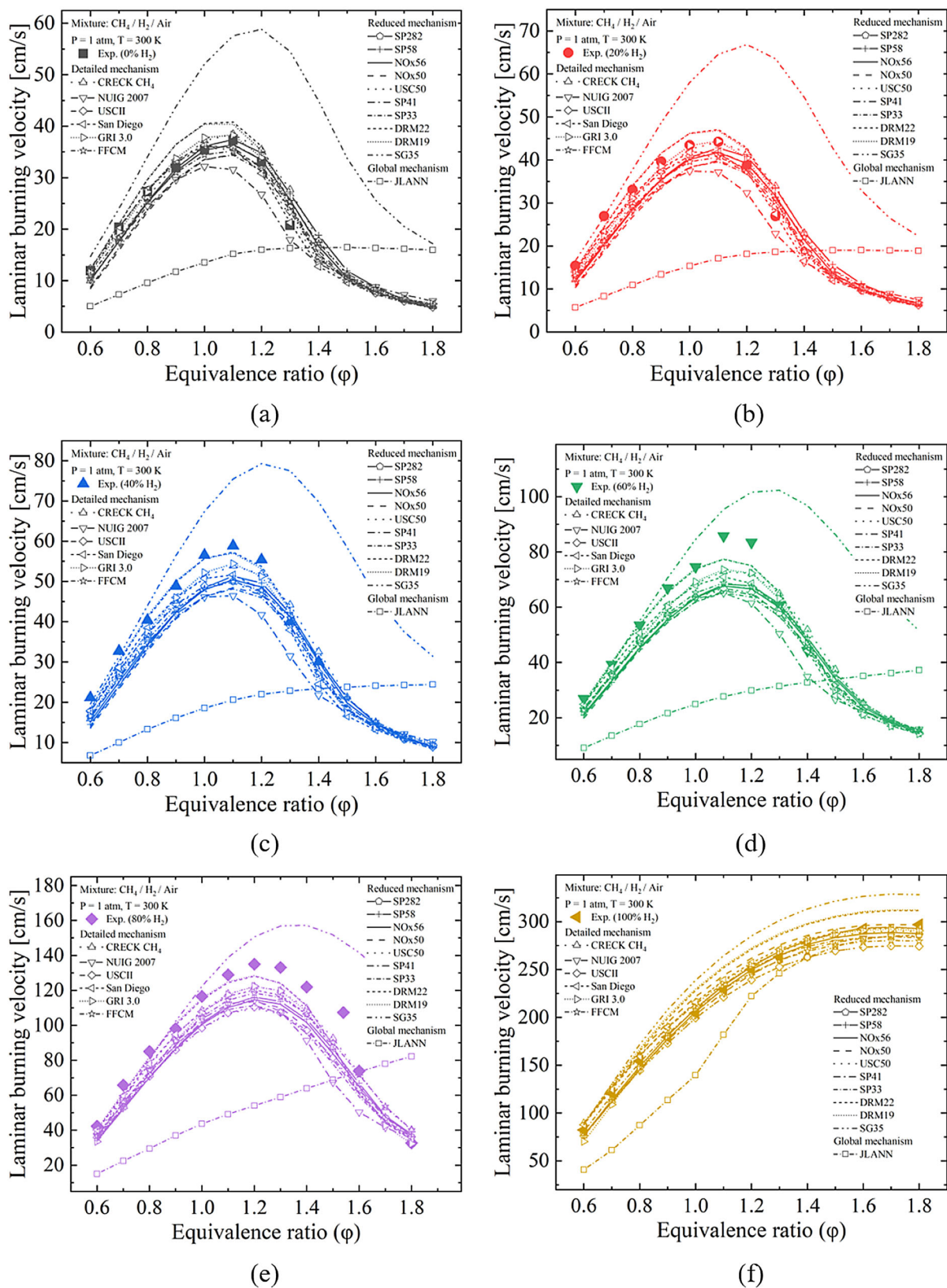


Fig. 11 Errors between predicted laminar burning velocity and experimental data for the H₂ blending ratios: **a** 0%, **b** 20%, **c** 40%, **d** 60%, **e** 80%, and **f** 100% at 1 atm as equivalence ratio increases. Symbols: experimental data; lines: calculated data in this work

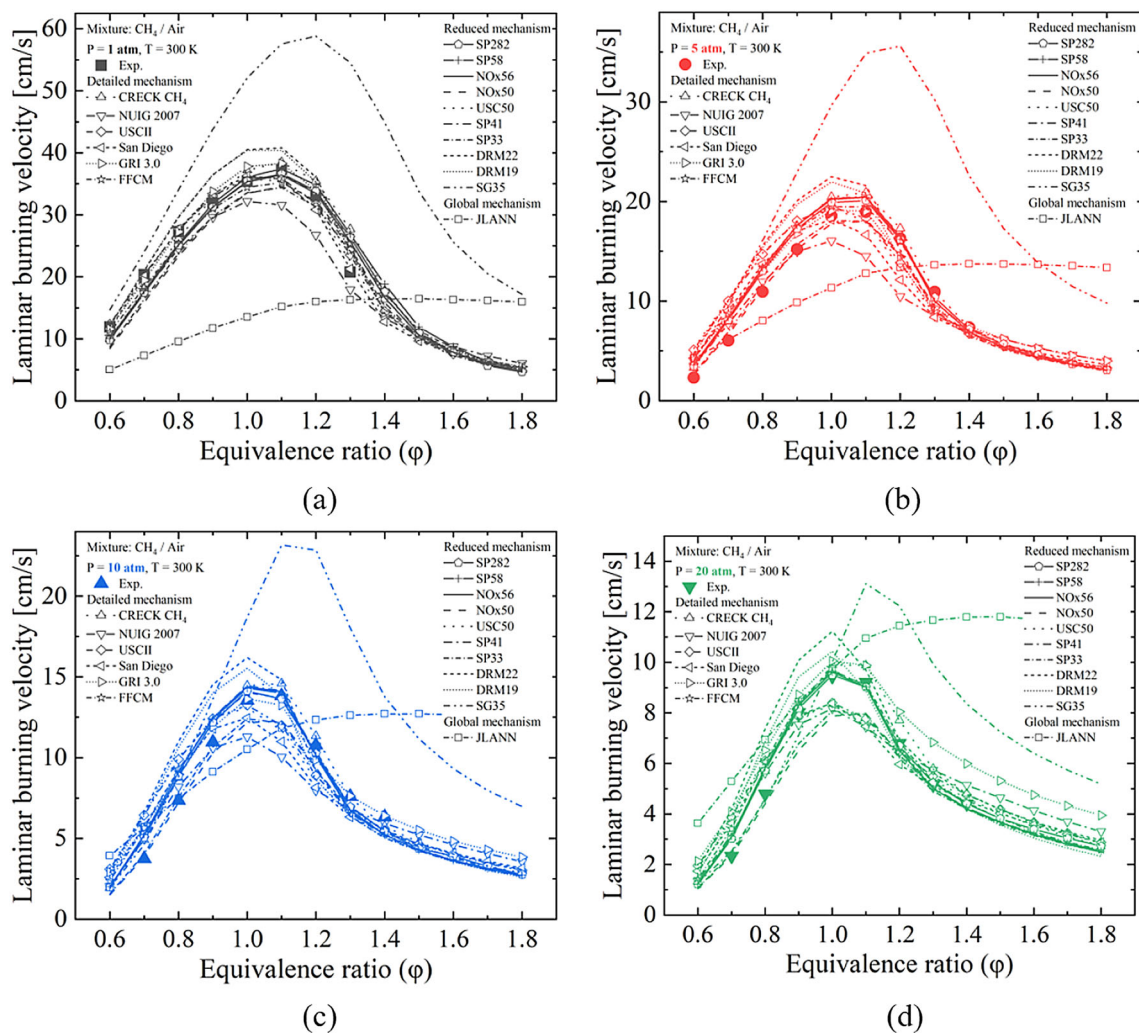


Fig. 12 Errors between predicted laminar burning velocity and experimental data for the combustion of methane and air at **a** 1 atm, **b** 5 atm, **c** 10 atm, and **d** 20 atm as equivalence ratio increases. Symbols: experimental data; lines: calculated data in this work

References

1. Yuze S, Tao C, Shahsavari M, Dakun S, Xiaofeng S, Dan Z, Bing W (2021) RANS simulations on combustion and emission characteristics of a premixed NH₃/H₂ swirling flame with reduced chemical kinetic model. *Chin J Aeronaut* 34:17–27. <https://doi.org/10.1016/j.cja.2020.11.017>
2. Ni S, Zhao D, You Y, Huang Y, Wang B, Su Y (2021) NO_x emission and energy conversion efficiency studies on ammonia-powered micro-combustor with ring-shaped ribs in fuel-rich combustion. *J Clean Prod* 320:128901. <https://doi.org/10.1016/j.jclepro.2021.128901>
3. Han HS, Han KR, Wang Y, Kim CJ, Sohn CH, Nam C (2022) Effects of natural-gas blending on ignition delay and pollutant emission of diesel fuel for the condition of homogenous charge compression ignition engine. *Fuel* 328:125280. <https://doi.org/10.1016/j.fuel.2022.125280>
4. Zhang B, Li Y, Liu H (2021) Ignition behavior and the onset of quasi-detonation in methane-oxygen using different end wall reflectors. *Aerosp Sci Technol* 116:106873. <https://doi.org/10.1016/j.ast.2021.106873>
5. Shokri M, Ebrahimi A (2018) Heat transfer aspects of regenerative-cooling in methane-based propulsion systems. *Aerosp Sci Technol* 82:412–424. <https://doi.org/10.1016/j.ast.2018.09.025>
6. Wang X, Fu J, Xie M, Liu Q, Liu J (2022) Numerical investigation of laminar burning velocity for methane–hydrogen–air mixtures at wider boundary conditions. *Aerosp Sci Technol* 121:107393. <https://doi.org/10.1016/j.ast.2022.107393>
7. Liang Y, Liu W (2018) Review and prospect of LOX/Methane rocket engine systems. *Aero Weaponry* 4:21–27. <https://doi.org/10.19297/j.cnki.41-1228/tj.2018.04.002>
8. Gascoïn N, Gillard P, Bernard S, Bouchez M (2008) Characterisation of coking activity during supercritical hydrocarbon pyrolysis. *Fuel Process Technol* 89:1416–1428. <https://doi.org/10.1016/j.fuproc.2008.07.004>
9. Dong C, Zhou Q, Zhang X, Zhao Q, Xu T, Se H (2010) Experimental study on the laminar flame speed of hydrogen/natural gas/air mixtures. *Front Chem Eng China* 4:417–422. <https://doi.org/10.1007/s11705-010-0515-8>
10. Zhang Y, Huang Z, Wei L, Niu S (2011) Experimental and kinetic study on ignition delay times of methane/hydrogen/oxygen/nitrogen mixtures by shock tube.

- Chin Sci Bull 56:2853–2861. <https://doi.org/10.1007/s11434-011-4635-4>
11. Zhang Y, Huang Z, Wei L, Zhang J, Law CK (2012) Experimental and modeling study on ignition delays of lean mixtures of methane, hydrogen, oxygen, and argon at elevated pressures. *Combust Flame* 159:918–931. <https://doi.org/10.1016/j.combustflame.2011.09.010>
 12. Han W, Dai P, Gou X, Chen Z (2020) A review of laminar flame speeds of hydrogen and syngas measured from propagating spherical flames. *Appl Energy Combust Sci* 1–4:100008. <https://doi.org/10.1016/j.jaecs.2020.100008>
 13. Zhang Y, Fu J, Shu J, Xie M, Liu J (2020) A chemical kinetic investigation of laminar premixed burning characteristics for methane-hydrogen-air mixtures at elevated pressures. *J Taiwan Inst Chem Eng* 111:141–154. <https://doi.org/10.1016/j.jtice.2020.04.013>
 14. Mitu M, Razus D, Schroeder V (2021) Laminar burning velocities of hydrogen-blended methane–air and natural gas–air mixtures, calculated from the early stage of p(t) records in a spherical vessel. *Energies* 14:7556. <https://doi.org/10.3390/en14227556>
 15. Shu B, Vallabhuni SK, He X, Issayev G, Moshhammer K, Farooq A, Fernandes RX (2019) A shock tube and modeling study on the autoignition properties of ammonia at intermediate temperatures. *Proc Combust Inst* 37:205–211. <https://doi.org/10.1016/j.proci.2018.07.074>
 16. Han HS, Sohn CH, Han J, Jeong B (2021) Measurement of combustion properties and ignition delay time of high performance alternative aviation fuels. *Fuel* 303:121243. <https://doi.org/10.1016/j.fuel.2021.121243>
 17. de Persis S, Idir M, Molet J, Pillier L (2019) Effect of hydrogen addition on NO_x formation in high-pressure counter-flow premixed CH₄/air flames. *Int J Hydrogen Energy* 44:23484–23502. <https://doi.org/10.1016/j.ijhydene.2019.07.002>
 18. Park S (2021) Hydrogen addition effect on NO formation in methane/air lean-premixed flames at elevated pressure. *Int J Hydrogen Energy* 46:25712–25725. <https://doi.org/10.1016/j.ijhydene.2021.05.101>
 19. Wang Y, Sohn CH, Bae J, Yoon Y (2021) Prediction of combustion instability by combining transfer functions in a model rocket combustor. *Aerosp Sci Technol* 119:107202. <https://doi.org/10.1016/j.ast.2021.107202>
 20. Wang Y, Cho CH, Du J, Sohn CH (2022) Effects of recess length on combustion instability in a model chamber with a gas-centered swirl coaxial injector. *Aerosp Sci Technol* 130:107911. <https://doi.org/10.1016/j.ast.2022.107911>
 21. Zhang P, Zsély IG, Samu V, Nagy T, Turányi T (2021) Comparison of methane combustion mechanisms using shock tube and rapid compression machine ignition delay time measurements. *Energy Fuels* 35:12329–12351. <https://doi.org/10.1021/acs.energyfuels.0c04277>
 22. Ströhle J, Myhrvold T (2007) An evaluation of detailed reaction mechanisms for hydrogen combustion under gas turbine conditions. *Int J Hydrogen Energy* 32:125–135. <https://doi.org/10.1016/j.ijhydene.2006.04.005>
 23. Kumar PP, Kim K-S, Oh S, Choi J-Y (2015) Numerical comparison of hydrogen-air reaction mechanisms for unsteady shock-induced combustion applications. *J Mech Sci Technol* 29:893–898. <https://doi.org/10.1007/s12206-015-0202-2>
 24. Olm C, Zsély IG, Pálvölgyi R, Varga T, Nagy T, Curran HJ, Turányi T (2014) Comparison of the performance of several recent hydrogen combustion mechanisms. *Combust Flame* 161:2219–2234. <https://doi.org/10.1016/j.combustflame.2014.03.006>
 25. Olm C, Zsély IG, Varga T, Curran HJ, Turányi T (2015) Comparison of the performance of several recent syngas combustion mechanisms. *Combust Flame* 162:1793–1812. <https://doi.org/10.1016/j.combustflame.2014.12.001>
 26. Zettervall N, Fureby C, Nilsson EJK (2021) Evaluation of chemical kinetic mechanisms for methane combustion: a review from a CFD perspective. *Fuels* 2:210–240. <https://doi.org/10.3390/fuels2020013>
 27. Wu Y, Panigrahy S, Sahu AB, Bariki C, Beeckmann J, Liang J, Mohamed AA, Dong S, Tang C, Pitsch H (2021) Understanding the antagonistic effect of methanol as a component in surrogate fuel models: a case study of methanol/n-heptane mixtures. *Combust Flame* 226:229–242. <https://doi.org/10.1016/j.combustflame.2020.12.006>
 28. Zhou C-W, Li Y, O’connor E, Somers KP, Thion S, Keesee C, Mathieu O, Petersen EL, DeVerter TA, Oehlschlaeger MA (2016) A comprehensive experimental and modeling study of isobutene oxidation. *Combust Flame* 167:353–379. <https://doi.org/10.1016/j.combustflame.2016.01.021>
 29. Petersen EL, Kalitan DM, Simmons S, Bourque G, Curran HJ, Simmie JM (2007) Methane/propane oxidation at high pressures: experimental and detailed chemical kinetic modeling. *Proc Combust Inst* 31:447–454. <https://doi.org/10.1016/j.proci.2006.08.034>
 30. Song Y, Marrodán L, Vin N, Herbinet O, Assaf E, Fittschen C, Stagni A, Faravelli T, Alzueta MU, Battin-Leclerc F (2019) The sensitizing effects of NO₂ and NO on methane low temperature oxidation in a jet stirred reactor. *Proc Combust Inst* 37:667–675. <https://doi.org/10.1016/j.proci.2018.06.115>
 31. Wang H, You X, Joshi AV, Davis SG, Laskin A, Egolfopoulos F, Law CK (2007) USC Mech Version II. High-temperature combustion reaction model of H₂/CO/C₁–C₄ compounds. http://ignis.usc.edu/USC_Mech_II.htm
 32. Tao Y, Smith GP, Wang H (2018) Critical kinetic uncertainties in modeling hydrogen/carbon monoxide, methane, methanol, formaldehyde, and ethylene combustion. *Combust Flame* 195:18–29. <https://doi.org/10.1016/j.combustflame.2018.02.006>
 33. San Diego Mechanism web page MaAECR, University of California at San Diego (2016) Chemical-Kinetic Mechanisms for Combustion Applications. <http://combustion.ucsd.edu>
 34. Smith GP, Golden DM, Frenklach M, Moriarty NW, Eiteneer B, Goldenberg M, Bowman CT, Hanson RK, Song S, Gardiner WC Jr., Lissianski VV, Qin Z (2000) GRI-Mech 3.0. <http://combustion.berkeley.edu/gri-mech/version30/text30.html>
 35. Sun W, Chen Z, Gou X, Ju Y (2010) A path flux analysis method for the reduction of detailed chemical kinetic mechanisms. *Combust Flame* 157:1298–1307. <https://doi.org/10.1016/j.combustflame.2010.03.006>
 36. Glarborg P, Kee RJ, Grcar JF, Miller JA (1986) PSR: A FORTRAN program for modeling well-stirred reactors. Sandia National Laboratories, Livermore
 37. Lutz AE, Kee RJ, Miller JA (1988) SENKIN: A FORTRAN program for predicting homogeneous gas phase chemical kinetics with sensitivity analysis. Sandia National Labs, Livermore
 38. Sharma D, Mahapatra S, Garnayak S, Arghode VK, Bandopadhyay A, Dash SK, Reddy VM (2020) Development of the reduced chemical kinetic mechanism for combustion of H₂/CO/C₁–C₄ hydrocarbons. *Energy Fuels* 35:718–742. <https://doi.org/10.1021/acs.energyfuels.0c02968>
 39. Kazakov A, Frenklach M (1995) DRM22. <http://combustion.berkeley.edu/drm/>
 40. Kazakov A, Frenklach M (1995) DRM19. <http://combustion.berkeley.edu/drm/>
 41. Frenklach M, Wang H, Goldenberg M, Smith G, Golden D, Bowman C, Hanson R, Gardiner W, Lissianski V, Frenklach M (1995) An optimized detailed chemical reaction mechanism for methane combustion. GRI-Mech, Berkeley, CA, Report No. GRI-95/0058
 42. Wang H, Frenklach M (1991) Detailed reduction of reaction mechanisms for flame modeling. *Combust Flame* 87:365–370. [https://doi.org/10.1016/0010-2180\(91\)90120-Z](https://doi.org/10.1016/0010-2180(91)90120-Z)

43. Smoke MD, Giovangigli V (1991) Formulation of the premixed and nonpremixed test problems. In: Smoke MD (ed) *Reduced kinetic mechanisms and asymptotic approximations for methane-air flames*, 1st edn. Springer, pp 1–28
44. Bulat G, Fedina E, Fureby C, Meier W, Stopper U (2015) Reacting flow in an industrial gas turbine combustor: LES and experimental analysis. *Proc Combust Inst* 35:3175–3183. <https://doi.org/10.1016/j.proci.2014.05.015>
45. Jones W, Lindstedt R (1988) Global reaction schemes for hydrocarbon combustion. *Combust Flame* 73:233–249. [https://doi.org/10.1016/0010-2180\(88\)90021-1](https://doi.org/10.1016/0010-2180(88)90021-1)
46. Si J, Wang G, Li P, Mi J (2020) Optimization of the global reaction mechanism for MILD combustion of methane using artificial neural network. *Energy Fuels* 34:3805–3815. <https://doi.org/10.1021/acs.energyfuels.9b04413>
47. Mathieu O, Levacque A, Petersen EL (2013) Effects of NO₂ addition on hydrogen ignition behind reflected shock waves. *Proc Combust Inst* 34:633–640. <https://doi.org/10.1016/j.proci.2012.05.067>
48. Teng F (2014) *The effect of hydrogen concentration on the flame stability and laminar burning velocity of hydrogen–hydrocarbon—carbon dioxide mixtures*. University of Sheffield, Sheffield
49. Amirante R, Distaso E, Tamburrano P, Reitz RD (2017) Laminar flame speed correlations for methane, ethane, propane and their mixtures, and natural gas and gasoline for spark-ignition engine simulations. *Int J Engine Res* 18:951–970. <https://doi.org/10.1177/1468087417720018>
50. ANSYS Chemkin-Pro: Release 2022 R1. ANSYS, Inc., Canonsburg
51. Hughes K, Turányi T, Clague A, Pilling M (2001) Development and testing of a comprehensive chemical mechanism for the oxidation of methane. *Int J Chem Kinet* 33:513–538. <https://doi.org/10.1002/kin.1048>

Publisher's Note Springer Nature remains neutral with regard to jurisdictional claims in published maps and institutional affiliations.

Springer Nature or its licensor (e.g. a society or other partner) holds exclusive rights to this article under a publishing agreement with the author(s) or other rightsholder(s); author self-archiving of the accepted manuscript version of this article is solely governed by the terms of such publishing agreement and applicable law.